ISTITUTO NAZIONALE DI FISICA NUCLEARE

Sezione di Milano

INFN/BE-03/02
9 settembre 2003

A LASER PULSE SHAPER FOR THE LOW EMITTANCE RADIOFREQUENCY SPARC ELECTRON GUN

Simone Cialdi and Ilario Boscolo[1]

[1]University and INFN, via Celoria 16, 20133 Milano, Italy

Abstract

The generation of an electron beam in a 3 GHz radiofrequency gun with a very low emittance requires a photocathode driven by a 10 ps ultraviolet high energy pulse with a rise time minor than 1 ps. This pulse can be provided by a Ti:Sa laser system completed with a pulse shaper programmed for that task. We discuss the design of a 4f-grating-lens pulse shaper optimized for our long rectangular pulse and for the lowest sensitivity to alignment. The Acousto-Optic Programmable Dispersive Filter shaping system is briefly discussed..

PACS.: 42.65.Re, 07.05.Tp

Submitted to Nuc. Inst. Meth. A

Published by ***SIS–Pubblicazioni***
Laboratori Nazionali di Frascati

1 Introduction

The development of low-emittance (few π mm-mrad) electron sources is required for application in X-ultraviolet (UV) free electron lasers (FELs) [1–3], Compton scattering [4] and new generation of linear colliders [5]. The study of our SPARC [1] (Sorgente Pulsata e Amplificata di Radiazione Coerente) FEL experiment has shown the necessity of an electron beam of $\approx 1\,\pi\,mm - mrad$ [6]. This requirement means a radiofrequency electron gun (rf-gun) whose photocathode is driven by a powerful rectangular pulse of 10 ps with a fraction of 1 ps rise time. In fact, it was shown also experimentally that the emittance depends on the temporal laser pulse characteristics and that its minimum value is reached with a rectangular pulse having the above written characteristics [7].

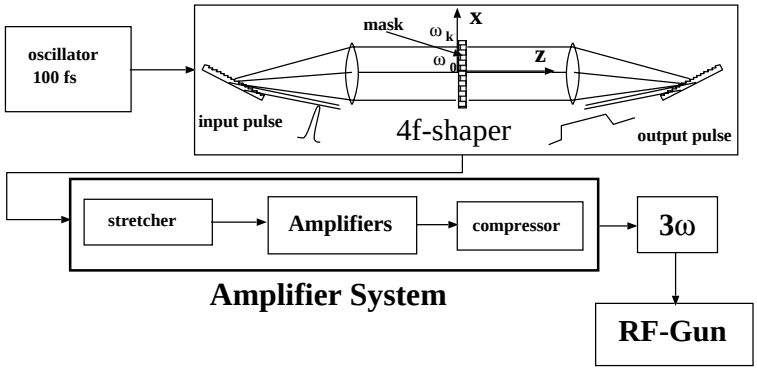

Figure 1: Sketch of the system layout with the pulse shaper insertion.

The generation of a rectangular light pulse is obtained by a laser system composed of an oscillator and a system of amplifiers with in between a temporal pulse shaper, as shown in Fig. 1. The proposed laser oscillator for the SPARC project is a cw Ti:Sapphire oscillator generating 100 fs long transform limited pulses at 73.9 MHz. A pulse shaping system set after the oscillator performs the transformation of that short pulse into the requested long rectangular pulse. A technology has been developed in the last decade for manipulating sub-picosecond pulses with the aim of generating ultrafast optical waveforms and relatively long square pulses according to user specifications [8–11]. Pulse shaping systems have already demonstrated a strong impact as experimental tools providing unprecedented control over ultrafast laser waveforms for ultrafast spectroscopy, nonlinear fiberoptics, and high-energy field physics. We propose to use that technology for stretching a short pulse into a long pulse with a rectangular shape and a very short rise time.

The physics principle of the pulse shaping is the spectral and amplitude modulation of the pulse spectral components. The shaping systems proposed so far with a

certain success are [9]: i) The Liquid Crystal Programmable Spatial Light Modulator, called LCP-SLM, ii) the acoustic-optic modulator Programmable Spatial Light Modulator (AOM-PSLM) [12], iii) the Acousto-Optic Programmable Dispersive Filter (AOPDF) [10,11] and iiii) movable and deformable mirrors (MM and DM) [9]. We will treat here the two i) and iii) systems because they demonstrated features of reliable and flexible operations and, furthermore, they are going to be tested in the SPARC experiment. They are based on different physics processes and, thus, different technologies. In this article we address more attention to the LCP-SLM shaper. The design parameters are discussed in view of the system sensitivity to their perturbation.

2 General consideration on pulse shaping

The field of a light pulse has, in the time domain, the expression

$$\tilde{E}(t) = E(t) \cdot e^{-i\,\omega_0 t} \qquad\qquad E(t) = \sqrt{I(t)} \cdot e^{+i\,\phi(t)} \tag{1}$$

The field in the frequency domain becomes

$$E(\omega) = \sqrt{I(\omega)} \cdot e^{-i\,\Phi(\omega)} \tag{2}$$

The spectral components of the light pulse have a delay time with respect the central frequency ω_0

$$\tau(\omega) = d\Phi(\omega)/d\omega \tag{3}$$

dependent on the frequency ω.
In general, the pulse manipulation occurs through the modulation, by the shaper, of the phase $\Phi(\omega)$ (therefore, of the time delay $\tau(\omega)$) and the modulation of $I(\omega)$.

The pulse shaping is a linear filtering process. In the time domain the filter action of the shaper is represented by the *impulse response function* $h(t)$, while in the frequency domain the filter action is represented by the Fourier transform $H(\omega)$ of $h(t)$. The output waveform $e_{out}(t)$ is the convolution of the input waveform $e_{in}(t)$ and the impulse response function h(t)

$$e_{out}(t) \;=\; h(t) * e_{in}(t) \tag{4}$$

In the frequency domain we may write

$$E_{out}(\omega) \;=\; H(\omega)\cdot E_{in}(\omega) \tag{5}$$

In general $H(\omega)$ will be a function of the type

$$H(\omega) = T(\omega)\cdot e^{i\psi(\omega)} \tag{6}$$

hence, the output will be

$$E_{out}(\omega) = T(\omega)\sqrt{I_{in}(\omega)}\cdot e^{i\,[-\psi(\omega)+\Phi_{in}(\omega)]} \tag{7}$$

The appropriate amplitude $T(\omega)$ and phase $\psi(\omega)$ modulation functions will provide any kind of output signal.

In our SPARC system the output laser pulse would have to be rectangular. The spectral components of the short pulse provided by the driving oscillator are delayed in time one another and possibly modulated in amplitude within the shaping system. We consider first the most direct case of a linear delay time

$$\tau(\omega) = \frac{d\Phi(\omega)}{d\omega} = b\,\omega. \tag{8}$$

This case is appropriate to AOPDF system, but it also enlightens the physics of the amplitude modulation and of phase modulation. Because of the linear delay the phase function will be

$$\Phi(\omega) = \int_0^{\omega} b\,\omega\,d\omega = \frac{1}{2}b\,\omega^2. \tag{9}$$

The output signal, given by the backward-Fourier transform, is

$$E_{out}(t) = \frac{1}{2\pi}\int_{bandwidth}\sqrt{I_{in}(\omega)}\,e^{-i\,\Phi(\omega)}\,e^{i\,\omega t}d\,\omega \tag{10}$$

We refer the calculations to the input signal of the Ti:Saffire oscillator and we keep the spectral bandwidth of $25\,rad/ps$ about the central frequency. The results are shown in Fig.2.

Frame (1a) shows the considered delay interval of 10 ps and the frequency window. Frame (1b) shows that the 100 fs input pulse is transformed into a 10 ps wide pulse with a rise time about 1 ps. The spectral components are spread over a time interval, therefore the pulse is chirped.

Frame (2b) shows that with a delay time function having two flat segments at the extremities the rise time is shortened: The wider the flat extremities the faster results the rise

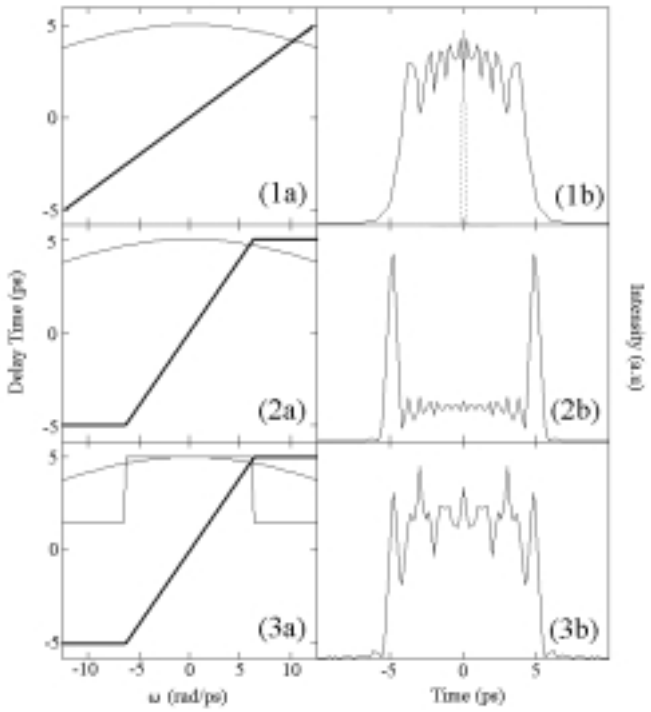

Figure 2: The $\tau(\omega)$ functions (bold lines) are depicted in left Frames. The curved thin lines on the top represent the section of the Gaussian spectrum used for the calculations. The bottom Frame (3a) shows also the transmission function (the rectangle with the two sides) having a reduced value at the extremities. In Frames (b) the computer calculated output pulse shapes relative to the different τ curves are reported. The amplitude modulation shown in the bottom frame is able to get rid of the overshoots (due to the superposition of the components without any delay).

time and the higher are the overshoots. The components relative to the flat segments add up in phase. To get round of the overshoots we must lower the amplitude of the relative components reducing the transmission for those spectral components, as shown in Frame (3a).

3 The LCP-SLM system

In this section we present the operation principle of the system, the components, the relative arrangement and finally we discuss the sensitivity of the system to the physical parameters.

3.1 The operation principle of the LCP-SLM system

The operation of a LCP-SLM shaping system is based on the filtering of the input pulse in the frequency domain. The procedure is: a) decompose spatially the frequency components of the input pulse, b) transform the dispersed rays in spots in a transform plane c) filter the spots (the frequency components), d) transform back the component rays in a convergent pulse and e) recombine (synthesize) the components in a pulse. These operations are made by *a 4f-setup with the filter mask in the center* as shown in Fig. 1. The light polarization at the grating and the mask are perpendicular one another, hence a waveplate for 90^o polarization rotation is inserted in between.
A first grating disperses angularly the individual frequency components with a linear law, at zero approximation,

$$x \simeq \alpha\omega \qquad \text{referred to the central frequency } \omega_0 \tag{11}$$

see Fig. 3. The first lens does the Fourier transformation of the dispersed beam onto the transform plane (the focal plane). The mask does the filtering. The second lens does the Fourier anti-transform. The second grating does the synthesis of the frequency components. The output pulse shape is given by the Fourier transform of the patterned mask, see Fig. 4, transferred onto the spectrum. The system is a zero time-dispersion line.

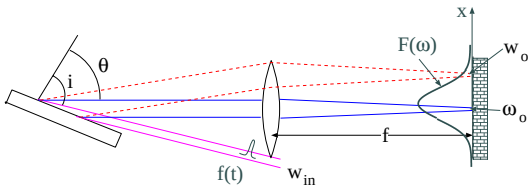

Figure 3: Angles and trajectories in the SLM. The spectral components of the input light beam are separated by the grating and focused at the mask by a lens with a beam waist w_0. The pulses are gaussian both in space and in time.

The field just after the mask will be (in the frequency domain, following Eqs. (4) and (5))

$$E_{out}(x,\omega) \sim H(x)\, E_{in}(\omega)\, e^{-\frac{(x-\alpha\omega)^2}{w_0^2}} \tag{12}$$

We notice that the linear relation between the coordinate x and the frequency ω allows the simple relation between the filter function $H_{SLM}(\omega)$ and the physical mask function $H_{SLM}(x)$ (the complex transmittance of the mask). From the general Eq. 5 combined with Eq. 12 and assuming a filtering action which allows only the lowest Hermite-Gaussian mode, we get for the filter function $H(\omega)$ [13]

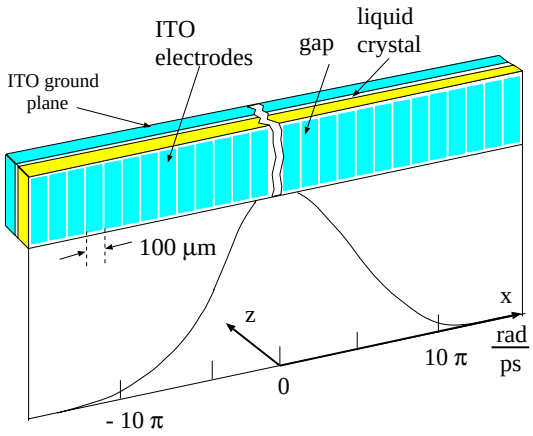

Figure 4: Schematic diagram of an electronically addressed, phase-only LCP-SLM.

$$H(\omega) = \sqrt{\frac{2}{\pi\, w_0^2}} \int_{mask} H_{SLM}(x)\; e^{-2\,\frac{(x-\alpha\omega)^2}{w_0^2}}\, dx \tag{13}$$

The mask of a LCP-SLM shaping system is patterned as an array of pixels interleaved with small gaps. In the Jenoptic model SLM-S 640/12 chosen for our system the pixels are $97\,\mu m$ wide and the gaps are $3\,\mu m$ wide. Because of the mask pixellation, the mask filter function $H_{SLM}(\omega)$ is pixellated. Eq. 4 is changed into [14]

$$e_{out}(t) \;\cong\; \left[\sum_n h(t - n\,\frac{1}{\delta\nu}) * e_{in}(t)\right] \cdot \frac{sin(\pi\delta\nu\, t)}{\pi\delta\nu\, t}. \tag{14}$$

The spectral width $\delta\nu$ is relative to the individual pixel of width $\delta x = 2\pi\alpha\delta\nu$ where α is the spatial dispersion of the beam components. Negligibly small interpixel gaps and a focused spot size w_0 at the masking plane less than the pixel dimension are assumed for obtaining the expression (14). The result of the pixellation is to produce an output pulse which is the convolution of the input pulse not only with the desired impulse response function h(t), but also with a series of replica impulse response functions, $h(t - n\delta\nu^{-1})$, occurring at times $t = n\delta\nu^{-1}$. The entire result is weighted by a temporal window function, $sinc(\pi\delta\nu t)$, which has the first zeros at $t = \pm\delta\nu^{-1}$. However, in our problem of obtaining a square intensity pulse at UV, i.e. after the frequency multiplication, the lateral replica become vanishingly small, therefore negligible.

A complete LCP-SLM induces both phase and amplitude modulations. Hence, the general frequency response function $H_{SLM}(\omega)$ is characterized by its amplitude modulation $T(\omega)$ and spectral phase $\psi(\omega)$, that is

$$H_{SLM}(\omega) = T(\omega)\, e^{i\,\psi(\omega)} \tag{15}$$

However, since in our problem only the temporal intensity profile is requested, we have the degree of freedom of choosing phase-only filters. In fact, the time domain intensity (and amplitude) is specified but the temporal phases are free. Besides, the shaped pulse must be highly amplified (a high energy per pulse is required by a metallic photocathode in order to deliver the wanted one nano-Coulomb charge), hence it is important to have a large spectrum in order to have a pulse stretching long enough for avoiding avoid optics damage into the amplifiers [8].

3.2 The LCP-SLM system configuration

The grating and the spatial dispersion. The system configuration is mostly determined by the spatial dispersion α of Eq. (11). It is related to the system parameters by the relation

$$\alpha = \frac{\lambda_0^2 \, f}{d \, 2\pi \, c \, cos[\theta_d(\lambda_0)]} \tag{16}$$

In the above equation f is the focal length, λ is the wavelength, c is the speed of light, θ_d is the diffracted angle of the central frequency, see Fig. 3. The diffraction angle comes from the grating law $m\lambda = d(sin\,\theta_i + sin\,\theta_d)\; with\; m = 1$.
Looking for an efficient diffraction into the first order a small grating period d must be chosen. The grating period d should be as small as possible so to get a reasonably good space separation of the spectral components. The Ivon-Jobin grating with $d = 0.5\,\mu m$ and 2000 grooves/mm seems a good choice.
The parameter α remains fixed by the mask dimension Δx and the spectral bandwidth $\Delta\omega$ selected for the system, being $\alpha = \Delta x/\Delta\omega$. The chosen mask is 64 mm wide. The selected spectral portion has a width of $\Delta\omega = 30\,\pi$ rad/ps (see below). Therefore we get $\alpha = 0.68\,mm \cdot ps/rad$. Once fixed α, Eq. (16) relates the focal length to the input angle (through the grating law). Frame (a) of Fig. 5 depicts that relation. We looked at the variation of α with θ_i, see Frame (b) of Fig. 5, for making the trade-off between the focal length and the input angle. The goal is to have an enough low sensitivity of α to θ_i perturbations and an apparatus dimension (that is a focal length) not too large. We have decided for a focal length $f = 700\;mm$ and, thus, an input angle $\theta_i = 62.76^o$.

The mask and the beam waist. The response function, considering the finite number of pixels and the finite dimension of the beam waist w_0, has the expression [9,13]

$$H(\omega) = \sqrt{\frac{2\alpha^2}{\pi \, w_0^2}}\, H_{SLM}(\omega) * e^{-2\frac{\alpha^2}{w_0^2}\omega^2} \tag{17}$$

The filter function $H_{SLM}(\omega)$ is shaped with steps (640 steps as the number of pixels). The steps are smoothed by the convolution with the Gaussian envelope function

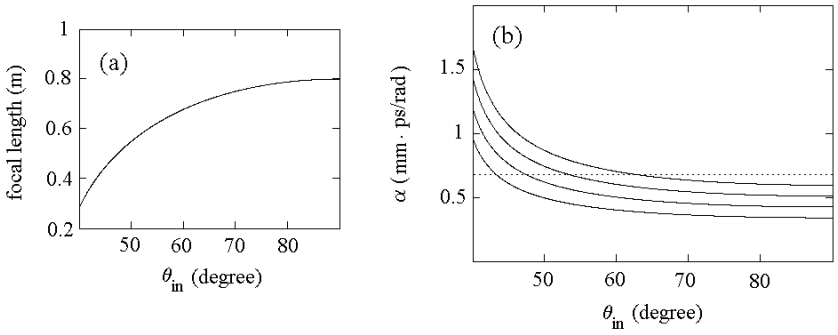

Figure 5: Frame (a) shows the curve of the focal length as function of the incident angle. Frame (b) shows the angular deviation as function of the incident angle θ_i for different focal lengths (in the order from the top 700, 600, 500 and 400 mm). The dotted line indicates the fixed value of $alpha$. The trade off between θ_i and f must be done: the longer the focal length the lower the sensitivity to θ_i perturbation. Willing a certain level of insensitivity to the input angle perturbation, that angle must be higher than 50^o. The dotted line in Frame (b) is the α value decided for our system.We remark that $\Delta\alpha/\alpha > O$ when $\Delta\theta_i < 0$ and viceversa. We would like to point out that with our $\theta_i \simeq 62,7^o$ the sensistivity of the system to θ_i variations is considerably less than the sensitivity at 50^o (taken as an example). Obviously, at this last incident angle the focal length would be different, see Fig. 5.

$e^{-2\,\alpha^2\omega^2/w_0^2}$ originated by the Gaussian spot of each spectral component at the mask. The smoothing effect is negligible when w_0 is minor than the pixel width. We have found, see next section, that for obtaining a long flat pulse, it is advisable to keep the beam waist smaller than the pixel dimension. In the simulations we have chosen $w_0 = 20\ \mu m$.
The beam waist w_0 of a spectral component at the mask as function of the system parameters results in

$$w_0 = \frac{cos\,\theta_i}{cos\,\theta_d} \cdot \frac{\lambda\, f}{\pi\, w_{in}} \tag{18}$$

where w_{in} is the waist of the input beam at the grating. Having fixed all the parameters but the input waist, this w_i must be 5.8 mm.

About the the spectral bandwidth $\Delta\omega$ the following consideration is in order: the frequency interval $\Delta\omega$ acts upon the rectangular pulse characteristics (that is rise time and plateau roughness) and the shaper dimensions. That bandwidth of $30\ \pi$ rad/ps results from the best trade-off among the three requirements of fast rise time, flat plateau and reduced mechanical dimensions .

In conclusion, in Fig. 6 the final design of the 4f-shaper for the SPARC machine is depicted.

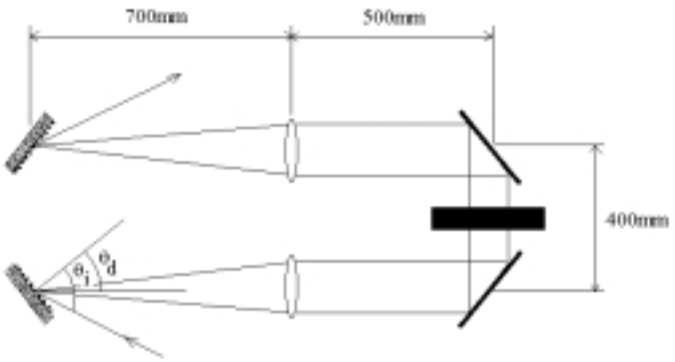

Figure 6: The schematic of the entire shaping system is depicted.

3.3 An LCP-SLM system with phase-only filtering

Choosing the phase-only filtering and the beam waist w_0 minor than the pixel dimension the spectral amplitudes of the input and output signals can be assumed the same. Therefore, $H_{SLM}(\omega) = exp[i\,\psi(\omega)]$. In this case an analytical solution does not generally exist, but many numerical solutions for the phase modulation function $\psi(\omega)$ satisfactory enough can be found. A computer assisted calculation can find a spectral phase distribution which leads to an output pulse which approximates fairly well the target pulse.
For the above purpose we have developed a computer program (in C++ language). The wanted transfer function H(x) of the programmable mask is found applying an iterative Fourier transform algorithm: the spectral pattern programmed into the pulse shaper is updated interactively according to a Genetic stochastic optimization Algorithm (GA) based on the difference between the desired and the wanted output (in an real system a measured output) [15,16]. The scheme of the adaptive algorithm is depicted in Fig. 7.

The complex spectral field $E(\omega)$ of the input pulse (characterized by its spectral amplitude and phase $A(\omega)$ and $\phi(\omega)$) and the temporal amplitude z(t) of the target pulse are given as inputs. The calculation begins by settings a zero phase delay to an initial trial phase vector Φ. In each iteration a random phase change $\delta\Phi_i$ is generated according to $\delta\Phi_i = R$ where R is a random variable uniformly distributed in the interval $-0.5 \div +0.5$ and the index i refers to the i-th pixel. At the end of each iteration a $cost - function$ provides a measure of the deviation of the output pulse from the target pulse. The new spectral phase function is accepted by the program if the $refreshed\,cost - function$ calculated with the new spectral phase function results smaller than that calculated with the last accepted spectral phase function. It is otherwise rejected. There are many kinds of $cost - functions$ and the choice of it is determined by the particular target waveform

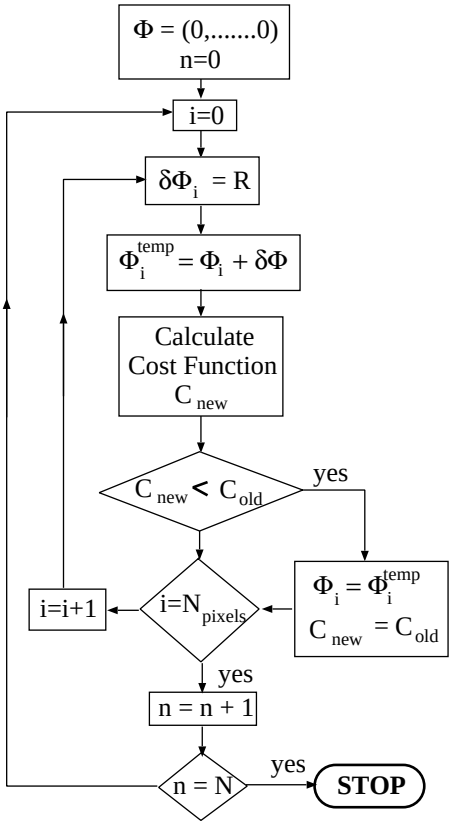

Figure 7: Scheme of the iterative Fourier transform algorithm (FT = Fourier Transform).

[16,17]. The stop of the iteration occurs when the value of the $cost - function$ arrives at its saturation. The final phase pattern $\Phi(\omega) - \psi(\omega)$ is transferred to the mask.
In our case of long rectangular pulse, the choice of the $cost - function$ came out to be very important [18]. The final chosen expression is $C = \int (I_n - I_n^{target})^2 dt$.
We have applied our simulation program, based on the genetic algorithm, to a mask of 640 pixels of 100 μm width illuminated by an input gaussian pulse of 100 fs. The trade-off among the parameters for the best result in terms of flatness at the third harmonic is: 0.5 ps rise time and $20\ \mu m$ for the beam waist at the mask. The result of simulations is depicted in Fig. 8.

It is satisfactory. We point out that the rise time and the plateau flatness resulted related: the shorter the rise time the worse the flatness. The system has shown a high sensitivity to variations of the input pulse length. It could be advisable to choose a less portion of the spectral bandwidth, so, in turn, to accept a worse flatness, for having a less sensitivity to small deviations of the pulse length.
We have done also simulations with an iterative Fourier Transform (Gerchberg-Saxton) algorithm [19]. The output simulated signal was remarkably worse than that obtained by

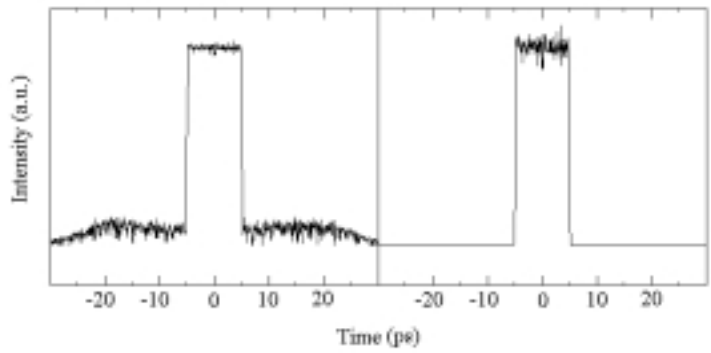

Figure 8: Simulated output pulses after the shaper obtained with the iterative algorithm: The signals of left and right frames refer to the fundamental harmonic and 3^{rd} harmonics respectively.

the computer program based on the Genetic algorithm.
We have checked the stability of the output pulse form versus the perturbation of the spatial dispersion, see Fig. 9. Frame (b) shows that the flatness variation with $\Delta\alpha/\alpha$ is slow.

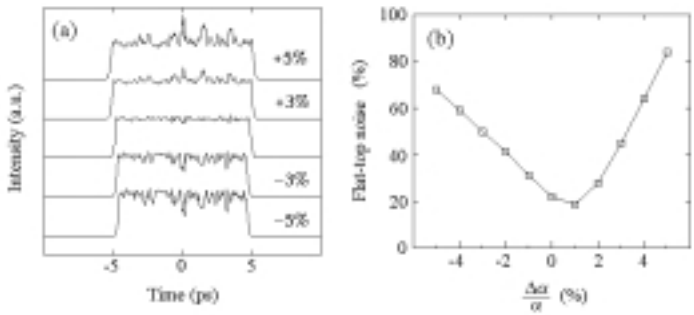

Figure 9: The curves of frame (a) show the variation of the signal plateau flatness for various value $\Delta\alpha/\alpha$. Frame (b) shows that a 20 % enhancement of the plateau roughness occurs for an angular dispersion variation of about 2 %. The Flat-top-noise was calculated by $(I_{max} - I_{min})/I_{average}$.

It is worth pointing out that a variation of α (because of the variations of θ_i) produces a variation of $\Delta\omega$ at the mask. This variation, in turn, produces a variation of the signal flatness. These considerations give reason of the previous discussion on the α sensitivity in relation to the focal length. Mathematically this relation comes out, from Eqs. (11) and (16), to be

$$\Delta\omega = \frac{\Delta x}{\alpha} = \Delta x \cdot d \cdot \frac{cos\,\theta_d}{2\pi\, c\, f}\omega_0^2. \tag{19}$$

In Fig. 10 we can see the relative variation of α for different percentage variations

on θ_i. From the top the four curves refer to the variations $4\%, 3\%, 2\% \, and \, 1\%$ respectively. To fix ideas, a variation of 2% on θ_i at the angle of 62.76^o induces a percentage variation on α of 1.5%. Anyway, from the curves we may conclude that the sensitivity of α to input angle variations at the considered focal length and input angle should not be a great problem.

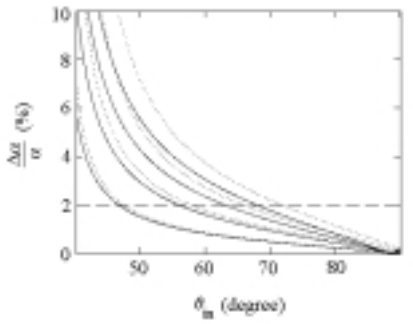

Figure 10: The curves show the sensitivity of the dispersion α for different relative variations of the input angle θ_i at the fixed focal length of 700 mm. From the top, the continuous lines refer to the following percentage variations: $4\%, 3\%, 2\% \, and \, 1\%$ respectively. Dotted lines refer to negative variations of θ_i. We notice that $\Delta\alpha/\alpha$ is not symmetric with respect the two side variations. We remark that $\Delta\alpha/\alpha > 0$ when $\Delta\theta_i < 0$ and viceversa. We would like to point out that with our $\theta_i \simeq 62, 76^o$ the sensistivity of the system to θ_i variations is considerably less than the sensitivity at 50^o (taken as an example). Obviously, at this last incident angle the focal length would be different, see Fig. 5.

4 The operation principle of the AOPDF system

The AOPDF system (called also DAZZLER) is based on the collinear acousto-optic interaction within a tellurium dioxide (TeO_2) crystal (acousto-optic modulator). An acoustic wave is launched into the crystal by a piezoceramic driven by an rf temporal signal. The acoustic wave, propagating with a certain velocity v_{ac} along the z-axis, sets a spatial wave within the crystal. A refractive index grating is created through the photoelastic effect. The grating period is $K = v_{ac}/\Omega$, where Ω is the radiofrequency drive frequency. The acousto-optic interaction can be either a bulk collinear or quasi-collinear interaction. Therefore the optical modes can be approximated by plane waves and the acousto-optic interaction is approximated within a waveguide or an optical fiber. In the propagation the transverse profile of the optical mode must be taken into account: different modes have different velocities. In a AOPDF each component of an incoming polarized mode 1, see Fig. 11, is diffracted into a mode 2 at the point $z(\omega)$ of the crystal where the resonance conditions

$$k_2 \simeq k_1 + K_s \qquad\qquad \omega_2 \simeq \omega_1 + \Omega \tag{20}$$

is matched. In the above equation k_1, k_2, and K_s are respectively the incident, the diffracted and the acoustic wavenumbers. The frequencies of the two optical waves are approximated equal. Since the velocities of the two modes are different, each component will cross the crystal length L in a different time $\Delta t(\omega)$. This $\Delta t = \tau(\omega)$ is proportional to $z(\omega)$. The spectral components of a short pulse are moved each other. The system behaves as a dispersive system where the group-velocity $v_g(\omega)$ has a significant value. The AOPDF can couple to the phase-filter an amplitude-filter modulating in amplitude the driving rf-signal. An acoustic wave variable in time and amplitude can provide control over the group delay and the amplitude of the diffracted spectral components.

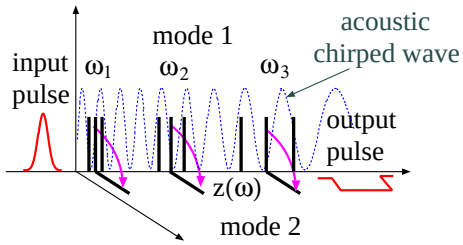

Figure 11: Schematic representation of the AOPDF principle. The acoustic wave and the optical incident and diffracted waves are collinear and propagating along the z-axis.

The tellurium dioxide (TeO_2) crystal of AOPDF has a typical 2.5-3 cm length in a quasi-collinear configuration. The two modes are polarized along the ordinary and extraordinary axes. At $\lambda = 800\,nm$, $n_1 = 2.226$ and $n_2 = 2.374$. The dispersion of the frequencies from 700 to 900 nm requires an rf frequency range between 40 to 60 MHz. The amplitude of the output, or diffraction efficiency, is controlled by the acoustic power.

Some comments on the LCP-SLM and Dazzler technologies are in order.

Dazzler is compact, it is simply set along along the system axis (it does not to have to be positioned in the Fourier plane of a dispersion line), it provides independent and simultaneous control of amplitude and phase modulation. These positive features of the Dazzler makes it very attractive. However, in practice a variety of factors, such as the transducer impedance matching, acoustic attenuation and nonlinearities could hamper the the possibility of a long crystal (that is the possibility of a large dispersion), lead to a low efficiency with expect the LCP-SLM. These drawbacks could sensibly lower the challenge of the device.

5 Notes on the other programmable shaping systems

We write some notes on the other shaping systems mentioned in the introduction for the sake of completeness.
In the AOM-PSLM system the mask is substituted by a AOM crystal, typically a TeO_2, driven by a radiofrequency (rf) voltage signal. This signal generates an acoustic wave traveling across the modulator with a velocity v_{ac}, leading to a refractive index grating through the photoelastic effect. The grating is phase and amplitude modulated through the rf wave modulation (see below). The spatially dispersed optical frequency components are diffracted by the grating, which is locally tuned to the components. The main drawbacks are the acoustic nonlinearities even at a level of rf power below that needed for reaching the full diffraction efficiency.
The movable mirrors system allows a pure phase simple modulation through a careful micro-position of a definite number of mirrors. The system does not have the requested flexibility.

6 Conclusions

A 4-f spatial light modulator with a programmable mask, phase-only shaped, looks like adequate for producing the target pulse of 10 ps with a rise time of less than 1 ps.

The Jenoptic model SLM-S 640/12 mask, used in the computer tests, showed to be suitable for the task of producing the requested rectangular pulse starting from the 100 fs pulse provided by the oscillator programmed for the laser system. The spectral pattern for the phase mask has been found with an home-made adaptive algorithm. The phase-only pulse shaping maintains the rise time of the input pulse. This result indicates that the input driving pulse could be as wide as 0.5 ps for the target pulse with a rise time of less than 1 ps.

The LCP-SLM system shows to have a relatively low sensitivity to alignment perturbations. We would also notice that the system is enough flexible to adapt the transfer function to changing user requests. For instance the change from a rectangular pulse shape to a ramp pulse shape can be done with a relatively low computational work.

References

[1] SPARC “Conceptual design of a high-brightness linac for soft X-ray SASE FEL source,” EPAC 2002 (La Villette, Paris) 5 June 2002.

[2] M. Cornacchia et al., “Linac coherent light source (LCLS) design study report” (Stanford University-University of California) Report No. SLAC-R-521/UC-414, revised 1998.

[3] F. Richard et al, “TESLA, the superconducting electron-positron linear collider with an integrated X-ray laser laboratory, technical design report,” Desy Report No. DESY2001-011, ISBN 3-935702-00-0, 2001

[4] P. T. Springer et al, “Ultrafast Material probing With the Falcon/Linac Thomson X-ray Source” 2002.

[5] J. Yang, M. Washio, A. Endo and T. Hori, Nuc. Inst. Methods Phys. Res. A **428** 556–569 (1999).

[6] M. Ferrario, M. Boscolo, V. Fusco, C. Vaccarezza, C. Roncisvalle, J. B. Rosenzweig and L. Serafini, “Recent advances and novel ideas for high brightness electron beam production based on photo-injectors,” In ICFA Workshop “The physics and application of high brightness electron beams” (Chia Laguna, Sardinia, Italy) 1–6 July 2002.

[7] J. Yang, F. Sakai, T. Yanagida, M. Yorozu, Y. Okada, K. Takasago, A. Endo, A. Yada, and M. Washio, J. Appl. Phys. **92,** 1608–1612 (2002).

[8] S. Backus, C. G. Durfee III, M. M. Murname and H. C. Kapteyn, Rev. Sci. Instrum. **69,** 1207–1223 (1998).

[9] A. M. Weiner, Rev. Sci. Instrum., **71,** 1929-1960 (2000).

[10] P. Tournois, Opt. Commun. **140,** 245–249 (1997).

[11] F. Verluise, V. Launde, J-P. Huignard, P. Tournois, and A. Migus, J. Opt. Soc. Am. B. **17,** 138–145 (2000).

[12] M. R. Fetterman, D Goswami, D. Keusters, W. Yang, J. K. Rhee, and W. S. Warren, Opt. Lett. **23**, 1843 (1998).

[13] R. N.Thurston, J. P. Heritage, A. M. Weiner and W. J. Tomlinson, IEEE J. Quantum Electron, **22,** 682-696 (1986).

[14] M. M. Wefers and K. A. Nelson, J. Opt. Soc. Am. B **127,** 1343–1362 (1995).

[15] D. Meshulach, D. Yelin, and Y. Silberberg, Opt. Commun. **138,** 345–348 (1997).

[16] D. Meshulach, D. Yelin, Y. Silberberg, J. Opt. Soc. Am. B **155,** 1615–1619 (1998).

[17] A. M. Weiner, S. Oudin, D. E. Leaird, D. H. Reitze, J. Opt. Soc. Am. B **105,** 1112-1120 (1993).

[18] S. Cialdi, I. Boscolo and A. Flacco, *Features of a phase-only shaper relative to a long rectangular ultraviolet pulse*, sent for pubblication.

[19] M. Hacker, G. Stobrawa and T. Feurer, Opt. Express **9**, 191 (2001).